Supporting Information

Inorganic Ligand-Protected Synthesis and Characterization of {Ag$_6$} Cluster within Annular Polyoxometalate

Yahao Sun, Shihao Zhang, Minzhen Cai, Pengtao Ma, Jingyang Niu* and Jingping Wang*

Henan Key Laboratory of Polyoxometalate Chemistry, College of Chemistry and Molecular Sciences, Henan University, Kaifeng Henan 475004 (P.R. China)

E-mail: jyniu@henu.edu.cn; jpwang@henu.edu.cn.

Table of Contents

Materials and Physical Measurements

All chemicals used in the reaction were purchased from commercial sources and were not further purified. The FT-IR spectra were collected on a Bruker VERTEX 70 IR spectrometer using KBr pellets in the region of 400–4000 cm^{-1}. Thermogravimetric analyses (TGA) were conducted using a NETZSCH STA 449 F5 Jupiter thermal analyzer in an N_2 atmosphere and the analysis was carried out over a temperature range of 25 °C to 800 °C with a heating rate of 10 °C·min^{-1}. Solid-state UV-vis absorption spectra and diffuse reflectance spectra were collected at room temperature using a HITACHIU-4500UV-Vis-NIR spectrometer equipped with a 60 mm diameter integrating sphere on a finely ground sample. Elemental analysis for Na, K, P, W, and Ag atoms was conducted by Inductively coupled plasma atomic emission spectrometer (ICP-OES) analyses and was recorded on a PerkinElemer Optima 2100 DV spectrometer (PerkinElmer, Waltham, MA). X-ray powder diffraction (PXRD) data were collected at room temperature using an X-ray powder diffractometer (Bruker, D8 Advance) with Cu Kα radiation (λ = 1.5418 Å) in the 2θ angular range of 5–50°. The X-ray photoelectron spectroscopy (XPS) technique was measured on a Thermo Scientific K-Alpha spectrometer with monochromatic Al K (hv = 1486.6 eV) as the excitation source at a working pressure of 12 kV. Cyclic voltammetry tests and the Mott-Schottky experiment were carried out on a CHI760E electrochemistry workstation (CH Instruments, Inc.) in a standard three-electrode system. The Ag/AgCl electrode and platinum foil were used as the reference electrode and counter electrode, respectively. Single-crystal X-ray diffraction data was collected at 150 K using graphite-monochromate Mo Kα radiation (λ = 0.71073 Å) on a Bruker D8 VENTURE PHOTON II. Alternating current (AC) impedance measurements were performed on a Pentium/IM6 impedance analyzer with frequencies ranging from 0.1 Hz to 5 MHz using an applied voltage of 50 mV. The relative humidity (RH) was controlled by a STIK Corp. CIHI-150B incubator. Water adsorption isotherm of compound **1** was tested on the Specific surface and porosity analyzer. The steady state photoluminescence spectra and time-resolved decay photoluminescence spectra were recorded on photoluminescence spectrometer (Edinburg FLS1000). The ^{1}H and ^{13}C spectra were obtained on a Bruker AVANCE NEO 500 MHz NMR spectrometer. The photocatalytic products were confirmed by GC−MS (Agilent 7890B GC/5973B MS, SE-54 capillary column), and GC calculations of conversion and selectivity were performed on Bruker 450-GC.

X-ray Crystallography

The crystal of compound **1** was mounted on a loop and maintained at 150 K during data collection using a Bruker D8 VENTURE PHOTON II CCD diffractometer with Mo Kα radiation (λ = 0.71073 Å). The structure was analyzed using Olex2 and solved with the ShelXT structure solution program. The direct methods were used to refine the text, which was then further refined using the ShelXL-2018/3 refinement package through least squares minimization.[1,2] In the final refinement, all the nonhydrogen atoms including W, Ag, P, K, and Na atoms were refined anisotropically.[3] Few lattice water molecules were located by Fourier difference maps; the rest lattice waters were positioned by TG analysis (Figure S4). In addition, serval protons were added to the structural formula to keep **1** electric neutrality, which is quite common in POM chemistry.[4] The crystallographic data of **1** has been deposited in the Cambridge Crystallographic Data Center with the CCDC number: 2349949. Detailed crystallographic data and structure refinement parameters are summarized in the following Table S1.

Synthesis of：Na$_6$K$_6$H$_{25}$[(P$_6$W$_{37}$O$_{127}$){Ag$_2$(Ag$_6$O$_{19}$)}]·53H$_2$O (1).

The solution of 0.5 M NaAC-HAc (pH=6) with CH$_3$COONa·3H$_2$O (34.02 g, 0.25 mol) dissolved in 500 mL

distilled water was slowly stirred until dissolved at ambient temperature. Subsequently, the pH of the solution was adjusted to 1.9 by adding nitric acid dropwise. And then taking out 10 mL reaction solution divided separately into reactors, $K_{12}[\alpha\text{-}H_2P_2W_{12}O_{48}]\cdot24H_2O$ (0.3 g, 0.063 mmol) was added under stirring conditions (pH=3.0). Once P_2W_{12} is dissolved, $AgNO_3$ (0.038 g, 0.22 mmol) is added, and a white suspension is obtained after stirring (pH=2.9). After stirring for a further 2 h, the resulting solution was sealed in a Teflon-lined stainless autoclave and heated at 80 °C for 96 h under autogenous pressure. After gently cooling to room temperature, the solution was filtrated into clean beakers and allowed to stand still for slow evaporation at room temperature. The colorless rod-like crystals **1** were obtained after two days with a yield of about 1.40 % based on $AgNO_3$. Anal. Calcd. (%) for **1**: Na, 1.12; K, 1.90, P, 1.51; W, 55.24; Ag, 7.01. Found: Na, 1.40; K, 1.36, P, 1.71; W, 56.39; Ag, 6.77. IR (KBr disks): 3471(m), 1618(m), 1381 (w), 1156 (s), 1086 (m), 920 (s), 825 (s), 712 (s).

Photoelectrochemistry property test of {Ag₆} semiconductor.

In the electrochemical workstation (CHI-760E, Shanghai, China), a three-electrode system was selected to measure the Mott−Schottky plot. In the three-electrode system, the glassy carbon electrode was employed as the working electrode, the Pt plate as the counter electrode, and the Ag/AgCl electrode as the reference electrode. The 0.2 M Na_2SO_4 solution was utilized as the electrolyte, and high-purity N_2 was introduced into the solution for a minimum of 30 minutes to remove oxygen prior to testing. The sample of 5 mg was dispersed into a mixture of 470 μL ethanol and 30 μL Nafion by sonication for 1 h. The suspension (20 μL) was applied to the surface of the working electrode and allowed to air dry naturally at room temperature.

The calculation of parameters for the assessment of catalyst performance.

The calculation of Turnover number (TON) and Turnover frequency (TOF):
$$TON = \frac{n_p}{n_c} \quad \text{and} \quad TOF = \frac{n_p}{n_c \cdot t}$$

where n_p is the molar amount of the product (mol); n_c is the molar amount of the catalyst (mol); t is the reaction time (h).

The calculation of apparent quantum yield (AQY): The AQY is determined using a similar method to that for the photocatalytic performance test. Catalyst 1 (0.5 μmol), nitrobenzene (0.5 mmol), $N_2H_4\cdot H_2O$ (3 mmol), methanol (1 mL), N_2 (1 atm), and 10 W 365 nm LED lamp. The intensity of the incident light was 14.93 mW·cm⁻², which was tested by a photometer (CEL-NP2000-2A, Beijing CEAulight Co., Ltd., China), and the irradiated area is 2 cm². The yield of aniline was 19.95% after 12 min.

$$AQY\% = \frac{amounts\ of\ products\ formed}{amounts\ of\ photons\ irradiated} \times 100\%$$

$$= \frac{N_e}{N_P} = \frac{nN_A/t}{IS/hv} = \frac{nN_A hc}{IS\lambda t} \times 100\%$$

N_e represents the amounts of products formed;

N_p represents the amounts of photons irradiated;

n is the molar amount of product formed (mol);

t is the reaction time (s);

N_A is Avogadro constant (6.022×10^{23} mol⁻¹);

I is the incident light intensity at a certain wavelength (W·m^{-2});

S is the irradiated area (m^2);

h is Planck constant (6.626×10^{-34} J·s);

c is the speed of light (2.998×10^8 m·s^{-1});

λ is the wavelength of incident light (m).
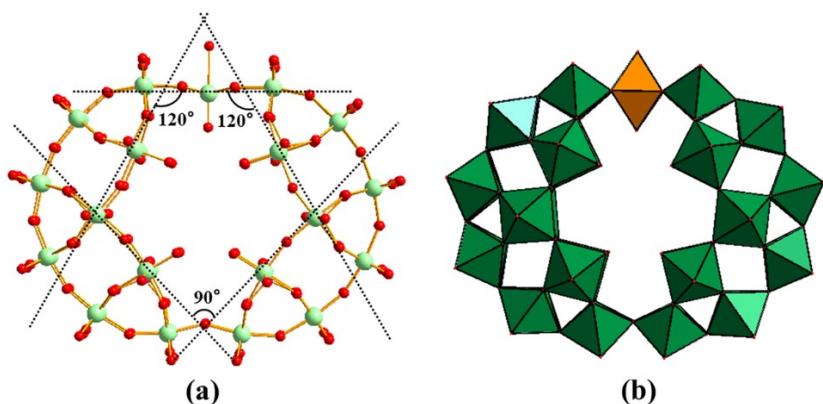
Figure S1. (a) The Ball-and-stick and (b) polyhedral representation of hollow ring for protected ligand {P_6W_{37}} of **1**. Color code: W (cyan), O (red), P (sky blue), WO_6 octahedron (green, orange).
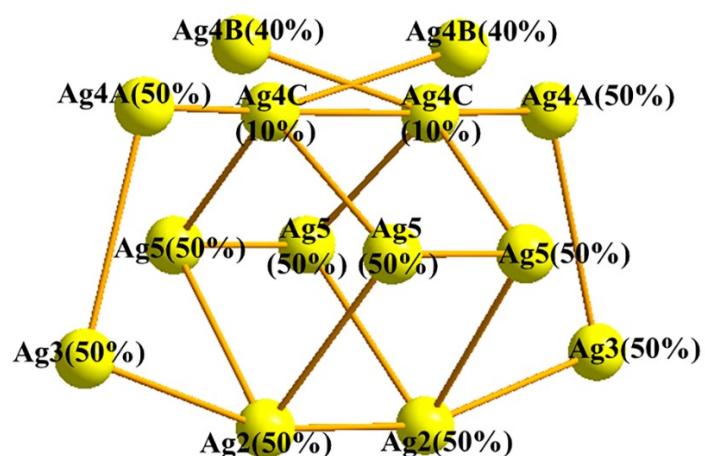
Figure S2. The details of disorder silver positions of compound **1**.
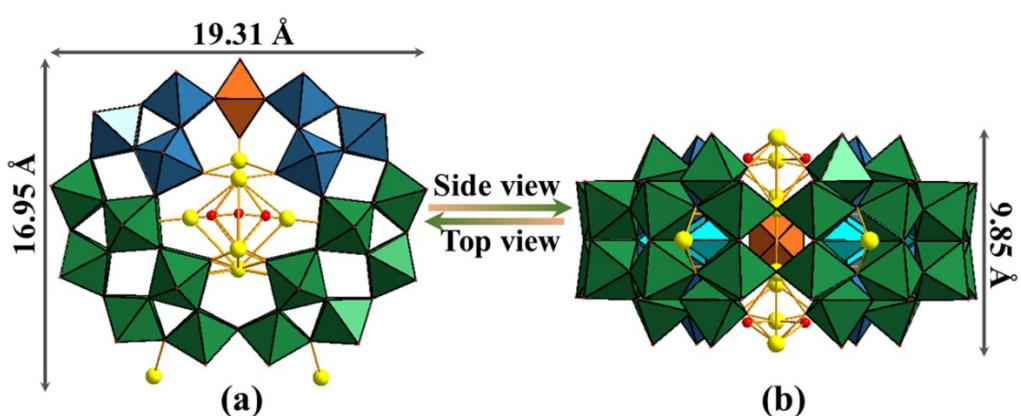
Figure S3. The polyhedral representation of compound **1** from (a) front view and (b) bottom view. Color code: Ag (yellow), O (red), PO_4 (sky blue), WO_6 octahedra (green, navy blue, and orange).
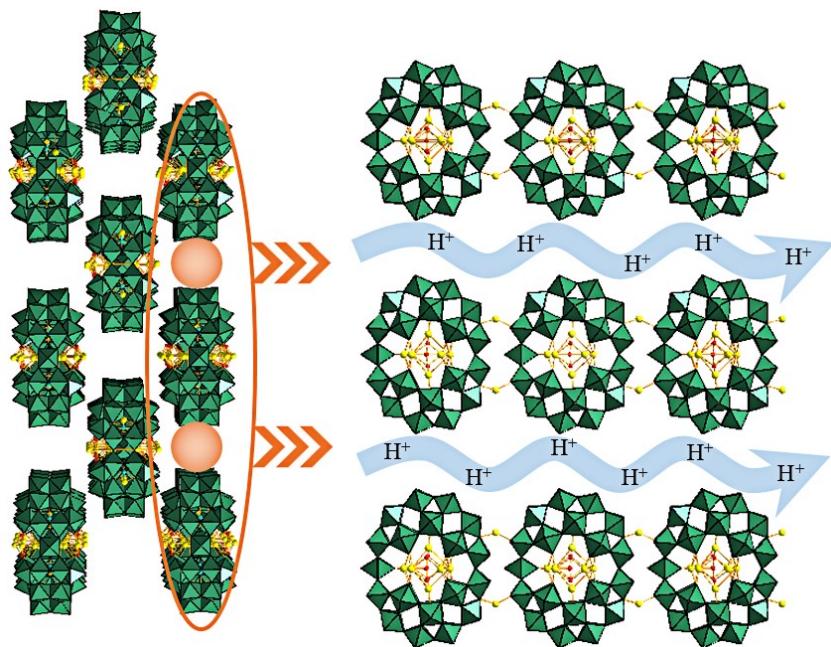
Figure S4. The plot of proton transport in compound **1**.

TG analysis: The TG measurement of compound **1** was made in an N_2 atmosphere flowing in the temperature range from 25 to 800 ℃ with a heating rate of 10 ℃·min^{-1}. As shown in Figure S5 (a), the result of TG analysis illustrates that compound **1** undergoes one-step weight loss. The total weight loss (8.31%) from the temperature 25 to 200 ℃ can be attributed to the loss of fifty-three lattice water molecules (calcd 8.26%).
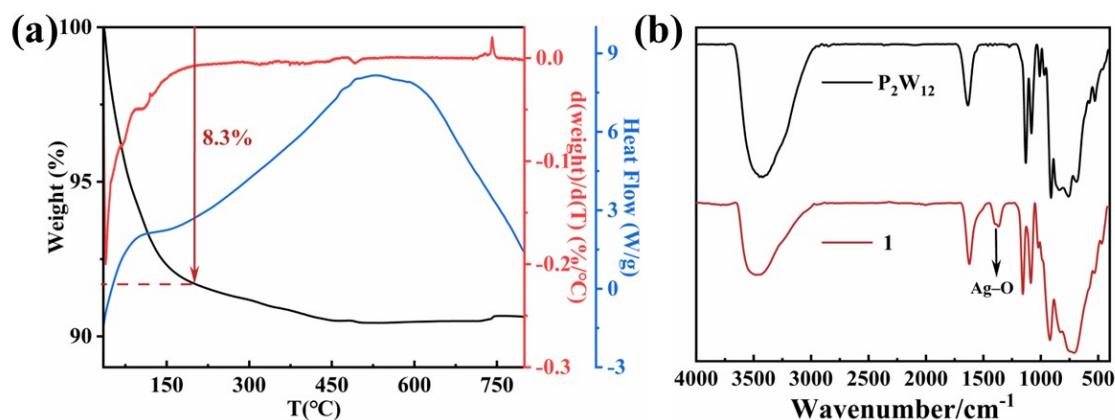
Figure S5. (a) The thermogravimetric curves of **1** and (b) the IR spectra of P_2W_{12} and compound **1**.
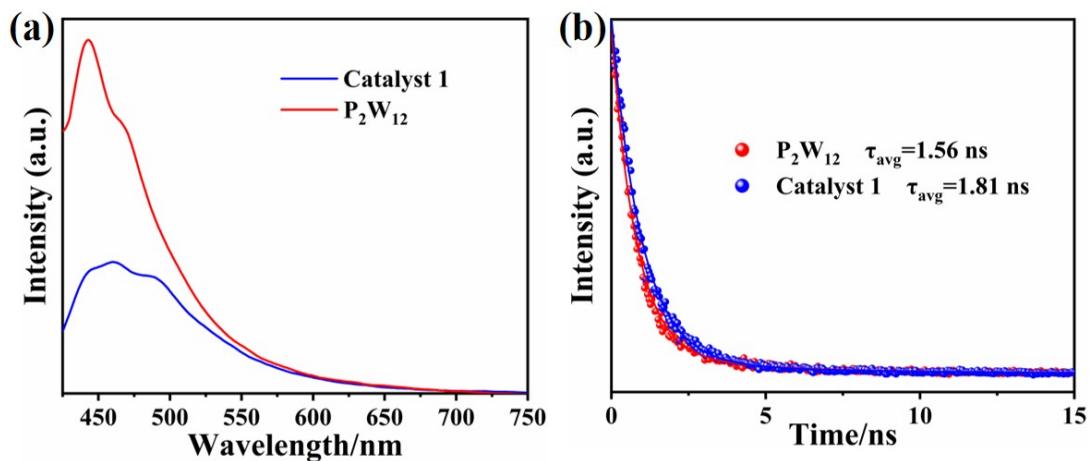
Figure S6. (a) PL and (b) TRPL plots of **1** and P$_2$W$_{12}$.
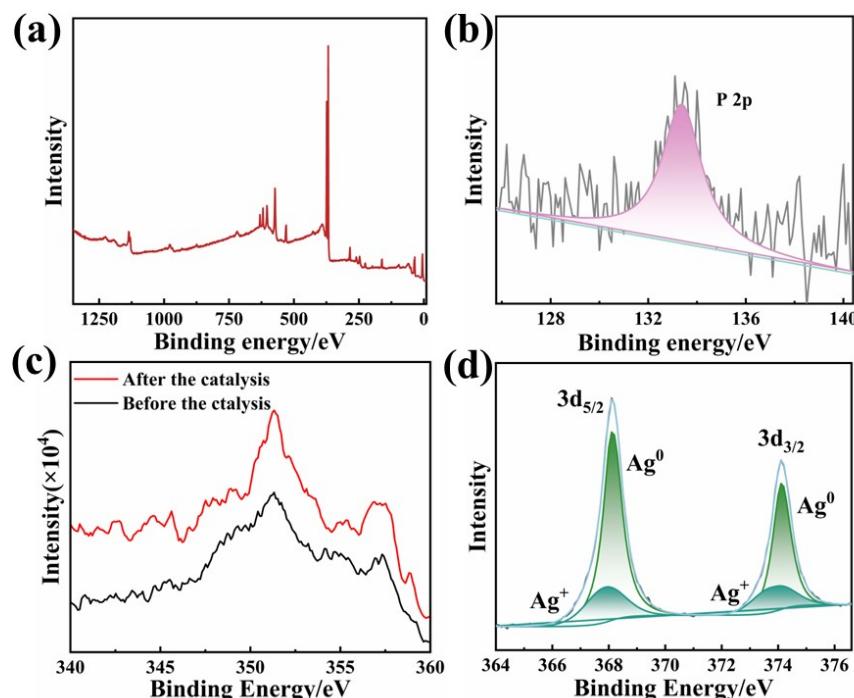
Figure S7. (a) The XPS survey spectra of compound **1**. (b) The XPS spectra of P 2p for **1**. (c) The Auger electron spectrum before and after catalysis. (d) XPS spectra of Ag 3d after catalysis.
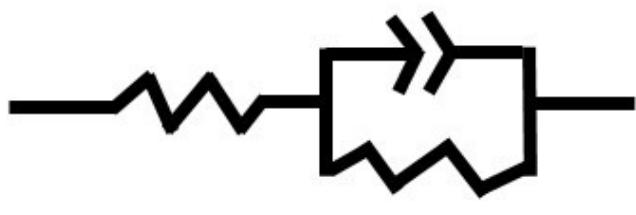
Rs (CPE-Rp)

Figure S8. The fitting equivalent circuit for measuring proton conductivity.
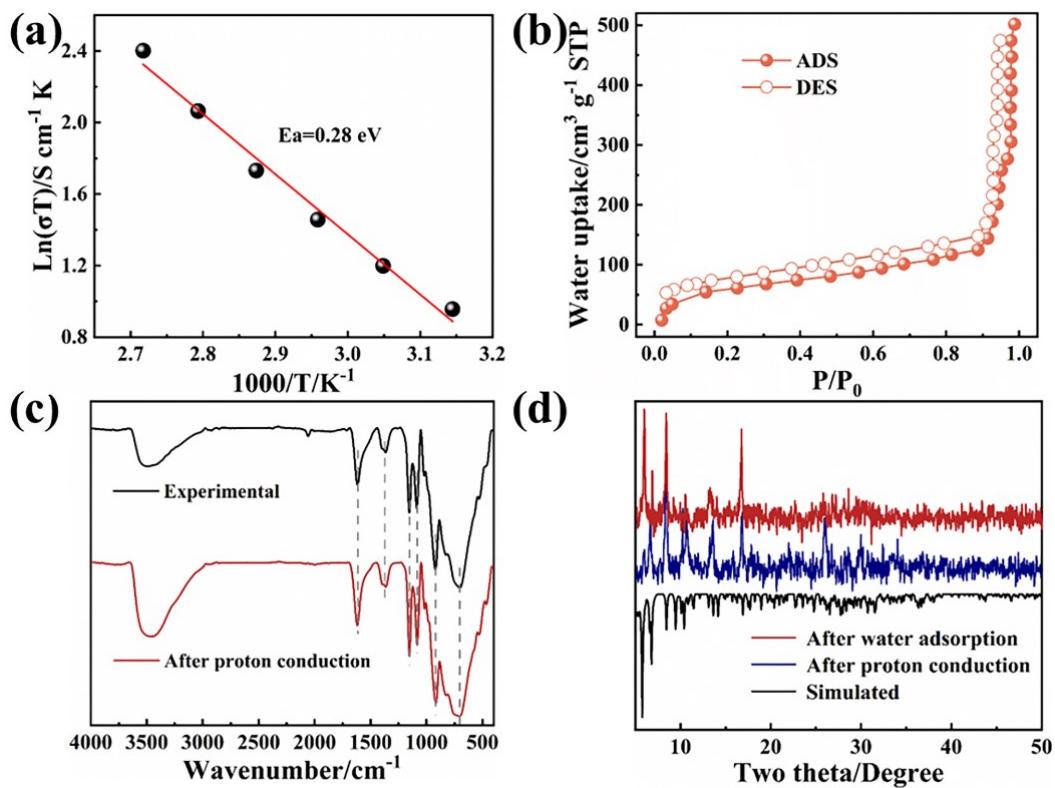
Figure S9. (a) Arrhenius plot of proton conductivities at 98% RH for **1**; (b) Water adsorption isotherm of **1**; (c) FTIR spectra of before and after test for **1**; (d) The PXRD of compound **1** with simulated and after water adsorption as well as after test.

Table S1. Crystallographic data parameters for **1**.

	1
Empirical formula	$Ag_8K_6Na_6O_{160}P_6W_{37}$
Formula weight	10783.77
Temperature (K)	150.0
Crystal system	orthorhombic
Space group	*Pmmn*
a /Å	20.9926(6)
b /Å	26.1232(6)
c /Å	17.5527(4)
α /deg	90
β /deg	90
γ /deg	90
V /Å^3	9625.8(4)
Z	2
ρ_{calc} /g cm^{-3}	3.721
μ /mm^{-1}	23.082
2θ range/deg	3.88 to 50.198
	$-24 \leq h \leq 25$
Index ranges	$-31 \leq k \leq 31$
	$-19 \leq l \leq 20$
Reflections collected	56317
Independent reflections	9000
R_{int}	0.0416
Data/restraints/parameters	9000/48/562
GOF on F^2	1.032
R_1, wR_2 [$I > 2\sigma(I)$]	0.0486, 0.1398
R_1, wR_2 [all data]	0.0537, 0.1453

$R_1=\Sigma||F_o|-|F_c||/\Sigma|F_o|$. $wR_2=\{\Sigma[w(F_o{}^2-F_c{}^2)^2]/\Sigma[w(F_o{}^2)^2]\}^{1/2}$

Table S2. The bond length of disorder position Ag−O and Ag−Ag.

Bond	Bond length	Bond	Bond length
Ag2−O27[2]	2.44 (11)	Ag3−O27[2]	2.118 (11)
Ag2−O27	2.44 (11)	Ag3−O27	2.118 (11)
Ag3−O1[2]	2.404 (14)	Ag4A−O1	2.371 (11)
Ag3−O1	2.404 (14)	Ag4A−O1[2]	2.371 (11)
Ag4A−O21	1.932 (11)	Ag4B−O21	2.420 (12)
Ag4A−O21[2]	1.932 (11)	Ag4B−O21[2]	2.420 (12)
Ag4B−O39	2.402 (11)	Ag4C−Ag5	3.222 (18)
Ag4C−Ag5[2]	3.222 (18)	Ag4C−Ag4C[1]	3.08(5)
Ag4C−O4W	1.77 (4)	Ag5−O4W	2.518 (5)
Ag5−O12	2.506 (10)	Ag2−Ag2[1]	3.067 (10)
Ag5−Ag5[3]	2.562 (7)		

Table S3. The bond length of ordered position W−O, Ag−O and the P−O.

Bond	Bond length	Bond	Bond length
Ag1−O4[3]	2.538 (10)	Ag1−O38	2.368 (16)
Ag1−O4	2.538 (10)	P1−O14	1.517 (9)
P1−O6	1.547 (13)	P2−O9	1.563 14)
P1−O5	1.556 (14)	P2−O20	1.534 (16)
P2−O12	1.52 (1)	P3−O16	1.534 (11)
P3−O35	1.571 (15)	W1−O17	1.778 (10)
P3−O26	1.558 (14)	W1−O8	1.942 (10)
W1−O14	2.194 (10)	W1−O22	1.909 (10)
W1−O10	2.037 (9)	W2−O4	1.95 (1)
W1−O31	1.741 (10)	W2−O13	1.931 (9)
W2−O6	2.272 (8)	W2−O10	1.840 (9)
W2−O17	1.735 (9)	W3−O3	1.923 (4)

W2−O2	1.938 (6)	W3−O5	2.281 (9)
W3−O4	1.943 (10)	W3−O8	1.874 (9)
W3−O7	1.940 (6)	W4−O30	1.731 (11)
W3−O18	1.722 (9)	W4−O25	1.962 (11)
W4−O28	1.881 (10)	W4−O15	1.977 (9)
W4−O22	1.886 (10)	W5−O11	1.930 (7)
W4−O12	2.16 (1)	W5−O15	1.863 (10)
W5−O13	1.897 (9)	W5−O23	1.729 (10)
W5−O19	1.949 (10)	W6−O1W	2.38 (2)
W5−O9	2.253 (9)	W6−O24[1]	1.914 (12)
W6−O24	1.914 (12)	W6−O24[3]	1.914 (12)
W6−O24[2]	1.914 (12)	W7−O16	2.153 (11)
W6−O39	1.71 (2)	W7−O28	1.92 (1)
W7−O21	1.799 (11)	W7−O34	1.937 (12)
W7−O29	2.045 (12)	W8−O20	2.277 (10)
W7−O40	1.752 (12)	W8−O32	1.928 (10)
W8−O25	1.867 (12)	W8−O41	1.731 (13)
W8−O33	1.925 (8)	W9−O26	2.281 (10)
W8−O19	1.917 (10)	W9−O32	1.886 (10)
W9−O29	1.824 (13)	W9−O37	1.930 (8)
W9−O36	1.982 (11)	W10−O42	1.729 (13)
W9−O43	1.718 (13)	W10−O35	2.261 (10)
W10−O34	1.883 (13)	W10−O38	1.944 (8)
W10−O36	1.881 (11)	W10−O24	1.942 (11)

Table S4. The angle value of ordered position O−W−O.

Mode	Angle	Mode	Angle
O8−W1−O10	81.5(4)	O8−W1−O14	82.7(4)
O10−W1−O14	81.4(3)	O22−W1−O8	162.5(4)
O22−W1−O10	86.8(4)	O22−W1−O14	82.7(4)
O27−W1−O8	94.4(4)	O27−W1−O10	166.1(4)
O27−W1−O14	85.0(4)	O27−W1−O22	93.9(4)
O31−W1−O8	96.2(5)	O31−W1−O10	93.6(4)
O31−W1−O14	175.0(4)	O31−W1−O22	97.5(5)
O31−W1−O27	100.0(5)	O2−W2−O4	87.6(5)
O2−W2−O6	72.1(4)	O4−W2−O6	82.8(4)
O10−W2−O2	157.6(4)	O10−W2−O4	87.7(4)
O10−W2−O6	85.6(4)	O10−W2−O13	91.4(4)
O13−W2−O2	88.5(5)	O13−W2−O4	167.5(4)
O13−W2−O6	84.6(4)	O17−W2−O2	99.7(5)
O17−W2−O4	95.5(4)	O17−W2−O6	171.6(4)
O17−W2−O10	102.6(4)	O17−W2−O13	96.9(4)
O3−W3−O4	164.7(5)	O3−W3−O5	82.1(5)
O3−W3−O7	89.4(6)	O4−W3−O5	82.7(4)
O7−W3−O4	88.6(5)	O7−W3−O5	73.3(4)
O8−W3−O3	88.8(5)	O8−W3−O4	87.4(4)
O8−W3−O5	84.9(4)	O8−W3−O7	158.1(4)
O18−W3−O3	97.4(5)	O18−W3−O4	97.9(4)
O18−W3−O5	172.4(4)	O18−W3−O7	99.1(5)
O18−W3−O8	102.7(5)	O15−W4−O12	83.4(4)
O22−W4−O12	83.5(4)	O22−W4−O15	89.7(4)
O22−W4−O25	165.8(4)	O25−W4−O12	83.2(4)

O25−W4−O15	84.0(4)	O28−W4−O12	83.9(4)
O28−W4−O15	166.9(4)	O28−W4−O22	92.3(4)
O28−W4−O25	91.0(4)	O30−W4−O12	177.1(4)
O30−W4−O15	94.2(4)	O30−W4−O22	98.3(5)
O30−W4−O25	94.8(5)	O30−W4−O28	98.3(5)
O11−W5−O9	72.8(4)	O11−W5−O19	88.2(5)
O13−W5−O9	84.8(5)	O13−W5−O11	89.9(5)
O13−W5−O19	166.8(4)	O15−W5−O9	86.4(4)
O15−W5−O11	159.0(4)	O15−W5−O13	90.4(4)
O15−W5−O19	86.8(4)	O19−W5−O9	82.2(5)
O23−W5−O9	171.8(4)	O23−W5−O11	99.2(5)
O23−W5−O13	97.4(4)	O23−W5−O15	101.5(4)
O23−W5−O19	95.8(5)	O24−W6−O1W	80.4(4)
O24[1]−W6−O1W	80.4(4)	O24[2]−W6−O1W	80.4(4)
O24[3]−W6−O1W	80.4(4)	O24[1]−W6−O24[3]	89.2(8)
O24−W6−O24[3]	87.6(8)	O24[1]−W6−O24[2]	87.6(8)
O24−W6−O24[2]	89.2(8)	O24[2]−W6−O24[3]	160.8(7)
O24−W6−O24[1]	160.8(7)	O39−W6−O1W	180.0
O39−W6−O24[3]	99.6(4)	O39−W6−O24[1]	99.6(4)
O39−W6−O24[2]	99.6(4)	O39−W6−O24	99.6(4)
O21−W7−O16	86.1(4)	O21−W7−O28	93.0(5)
O21−W7−O29	167.1(5)	O21−W7−O34	93.6(5)
O28−W7−O16	83.0(4)	O28−W7−O29	87.3(4)
O28−W7−O34	164.1(5)	O29−W7−O16	81.2(4)
O34−W7−O16	83.0(5)	O34−W7−O29	83.1(4)
O40−W7−O16	173.7(5)	O40−W7−O21	100.2(6)
O40−W7−O28	96.3(5)	O40−W7−O29	92.6(6)

|			
O40−W7−O34	96.7(6)	O19−W8−O20	82.4(5)
O19−W8−O32	165.8(5)	O19−W8−O33	88.7(6)
O25−W8−19	87.9(4)	O25−W8−O20	84.9(4)
O25−W8−O32	88.1(5)	O25−W8−O33	157.7(5)
O32−W8−O20	83.7(5)	O33−W8−O20	72.8(5)
O33−W8−O32	89.8(6)	O41−W8−O19	97.3(5)
O41−W8−O20	172.5(6)	O41−W8−O25	102.6(6)
O41−W8−O32	96.9(5)	O41−W8−O33	99.7(7)
O29−W9−O26	84.3(4)	O29−W9−O32	91.8(5)
O29−W9−O36	86.0(5)	O29−W9−O37	156.5(5)
O32−W9−O26	84.3(5)	O32−W9−O36	167.2(5)
O32−W9−O37	89.8(6)	O36−W9−O26	82.9(5)
O37−W9−O26	72.5(5)	O37−W9−O36	87.3(6)
O43−W9−O26	172.5(6)	O43−W9−O29	102.6(6)
O43−W9−O32	98.1(5)	O43−W9−O36	94.6(5)
O43−W9−O37	100.3(7)	O24−W10−O35	79.8(5)
O24−W10−O38	84.6(6)	O34−W10−O24	89.1(5)
O34−W10−O35	84.6(4)	O34−W10−O38	157.9(5)
O36−W10−O24	162.6(5)	O36−W10−O34	89.4(5)
O36−W10−O35	82.8(5)	O36−W10−O38	90.3(6)
O38−W10−O35	73.5(5)	O42−W10−O24	97.7(5)
O42−W10−O34	101.9(7)	O42−W10−O35	173.1(6)
O42−W10−O36	99.5(5)	O42−W10−O38	99.9(7)

Table S5. Bond valence sum calculations of ordered P, W and O atoms of compound **1**.

Atom Code	Bond Valence	Valence State	Atom Code	Bond Valence	Valence State
W1	6.218	+6	W6	6.068	+6
W2	6.072	+6	W7	6.113	+6
W3	6.047	+6	W8	6.125	+6
W4	6.097	+6	W9	6.264	+6
W5	6.161	+6	W10	6.120	+6
P1	5.001	+5	P2	5.008	+5
P3	4.808	+5	O2	1.890	-2
O3	1.968	-2	O4	1.999	-2
O5	1.928	-2	O6	1.971	-2
O7	1.885	-2	O8	2.057	-2
O9	1.962	-2	O10	1.956	-2
O11	1.931	-2	O12	1.984	-2
O13	2.018	-2	O14	1.781	-2
O15	2.005	-2	O16	1.778	-2
O17	1.635	-2	O18	1.698	-2
O19	1.915	-2	O20	2.011	-2
O22	2.109	-2	O23	1.662	-2
O24	1.943	-2	O25	2.030	-2
O26	1.921	-2	O28	2.094	-2
O29	1.993	-2	O30	1.653	-2
O31	1.609	-2	O32	2.058	-2
O33	1.957	-2	O34	2.044	-2
O35	1.925	-2	O36	1.941	-2
O37	1.931	-2	O38	1.854	-2
O40	1.562	-2	O41	1.658	-2
O42	1.667	-2	O43	1.712	-2

Table S6. Comparison of various proton conducting materials.

Compound	σ (S cm^{-1})	E_a (eV)	Conditions	Type
Compound 1	**3.00×10^{-2}**	**0.28**	**368 K, 98% RH**	**This work**
{Ce$_{11}$Mo$_{96}$}[5]	9.01×10^{-2}	0.38	353 K, 98% RH	
{Ln$_{10}$Ni$_{48}$}[6]	2.05×10^{-2}	0.22	295 K, 100% RH	
3D-{Mo$_{154}$}n[7]	1.10×10^{-2}	0.26	298 K, 100% RH	POMs
[P$_5$W$_{30}$]$_2$⊂{Mo$_{22}$Fe$_8$}[8]	1.70×10^{-2}	0.31	368 K, 90% RH	
{BiP$_5$W$_{30}$-PAA}[9]	1.70×10^{-3}	0.24	338 K, 75% RH	
Zr-TCPBP-HCl[10]	1.20×10^{-3}	0.17	341 K, 98% RH	
MFM-300(Cr)·SO$_4$(H$_2$O)$_2$[11]	1.26×10^{-2}	0.04	298 K, 99% RH	MOFs
H$_3$PO$_4$@NKCOF-54[12]	2.33×10^{-2}	0.29	433 K, anhydrous	
H@TPT-COF[13]	1.27×10^{-2}	0.17	433 K, anhydrous	COFs
HOF-FJU-36[14]	2.83×10^{-5}	0.66	323 K, 55% RH	
[(CN$_3$H$_6$)$_2$(C$_{10}$O$_8$H$_4$)] (GC-2)[15]	1.78×10^{-2}	0.46	298 K, 98% RH	HOFs

NKCOF=Nankai Covalent Organic Framework; FJU=Fujian Normal University

Table S7. Optimization of **1** for reduction of nitrobenzene to aniline [a]
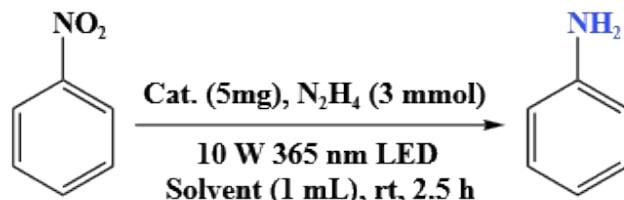
Entry	Catalyst (mg)	Solvent	Yield (%) [b]
1	5	CH$_3$OH	98.55
2	5	CH$_3$CN	10.26
3	5	CH$_3$CH$_2$OH	73.58
4	5	n-hexane	14.04
5	5	acetone	trace
6	5	CH$_2$Cl$_2$	49.99
7	5	methylbenzene	28.26
8	10	CH$_3$OH	94.85
9	2.5	CH$_3$OH	90

[a] **1** (5 mg), substrate (0.5 mmol), CH$_3$OH (1 mL), N$_2$H$_4$·H$_2$O (3 mmol), N$_2$ (1 atm), 10 W 365 nm LED lamp, rt, 2.5 h. [b] Determined by GC analysis.

Table S8. Summary of the yield of the reduction of nitrobenzene with different catalysts.

Entry	Catalyst	Temperature/°C	Light source	Hydrogen source	Time/h	Yield/%	Ref.
1	$Na_6K_6H_{25}[(P_6W_{37}O_{127})\{Ag_2(Ag_6O_{19})\}]\cdot53H_2O$	RT	365 nm	$N_2H_4\cdot H_2O$	2.5	98.55	**This work**
2	$Na_5H_{5.68}[Na_{0.17}Rh_{0.83}{}^{III}(C_6H_8N_2)_2Cl_2]_2(C_8H_8N_2)_2[As_4W_{40}O_{140}Rh_4{}^{IV}(C_6H_4N_2S)_2]\cdot nH_2O$	RT	Visiable light	$N_2H_4\cdot H_2O$	6	96	[16]
3	$Cs_4Na_2H_2[Te_2W_{20}O_{72}(H_2O)\{(C_6H_6)Ru\}_4]\cdot12H_2O$	RT	Visiable light	$N_2H_4\cdot H_2O$	6	99.8	[17]
4	ZnW-TPT	RT	365 nm	$N_2H_4\cdot H_2O$	6	99	[18]
5	Cu(I)-TPT	RT	365 nm	$N_2H_4\cdot H_2O$	8	99	[19]
6	CoW-TPT	RT	365 nm	TEOA	12	94.71	[20]
7	$1\text{-}Sb_8Mo_{18}$	80	/	$N_2H_4\cdot H_2O$	2	100	[21]

Table S9. The table of catalytic reduction of N-phenylhydroxylamine and azobenzene by **1**[a].

Entry	Substrate	Yield [b] (%)
1		43.88
2		-
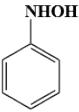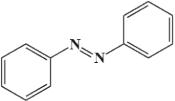
[a] Catalyst **1** (5 mg), substrate (0.5 mmol), CH_3OH (1 mL), $N_2H_4\cdot H_2O$ (3 mmol), N_2 (1 atm), a 10 W 365 nm LED lamp, rt, and 2.5 h. [b] Isolated yields.
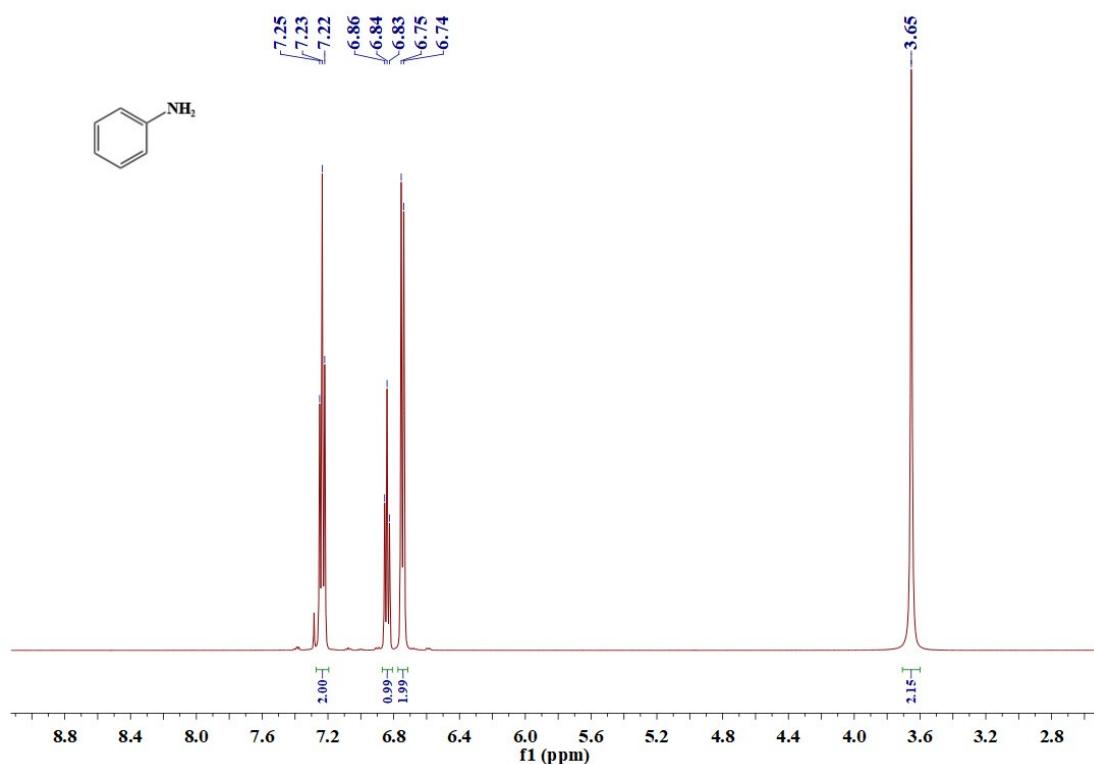
Figure S10. ¹H NMR spectra of **Aniline** (500 MHz, CDCl₃).

¹H NMR (500 MHz, CDCl₃) δ 7.23 (t, J = 7.7 Hz, 2H), 6.84 (t, J = 7.4 Hz, 1H), 6.75 (d, J = 8.1 Hz, 2H), 3.65 (s, 2H).
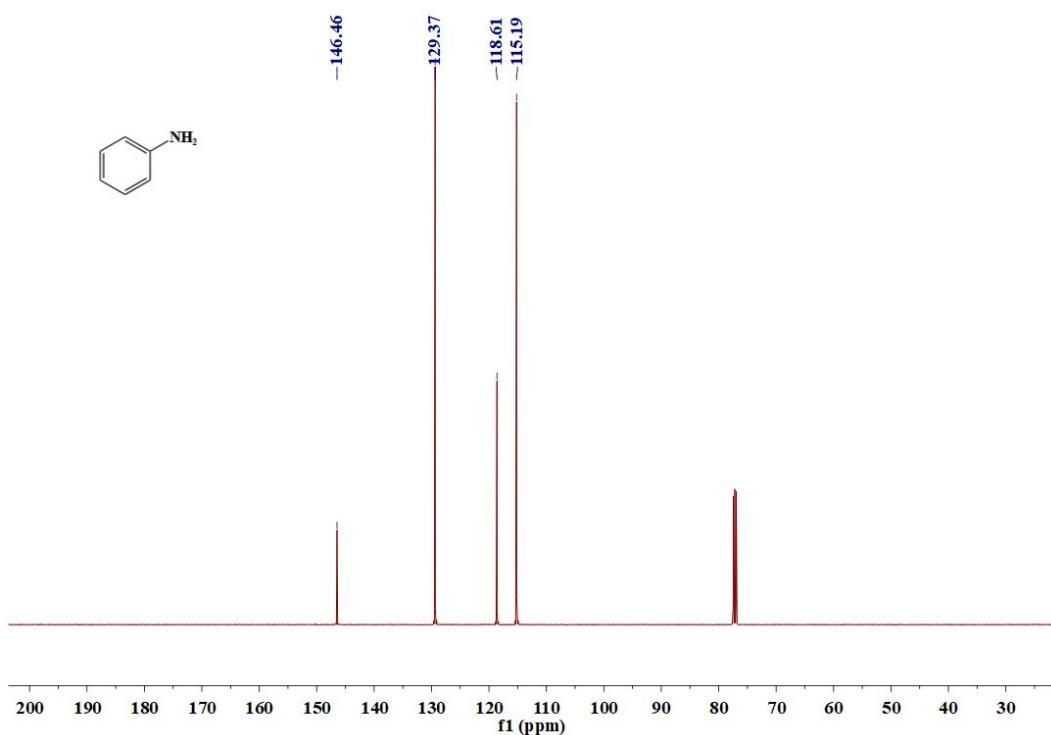
**Figure S11.** ¹³C NMR spectra of **Aniline** (126 MHz, CDCl₃).

¹³C NMR (126 MHz, CDCl₃) δ 146.46 (s), 129.37 (s), 118.61 (s), 115.19 (s).
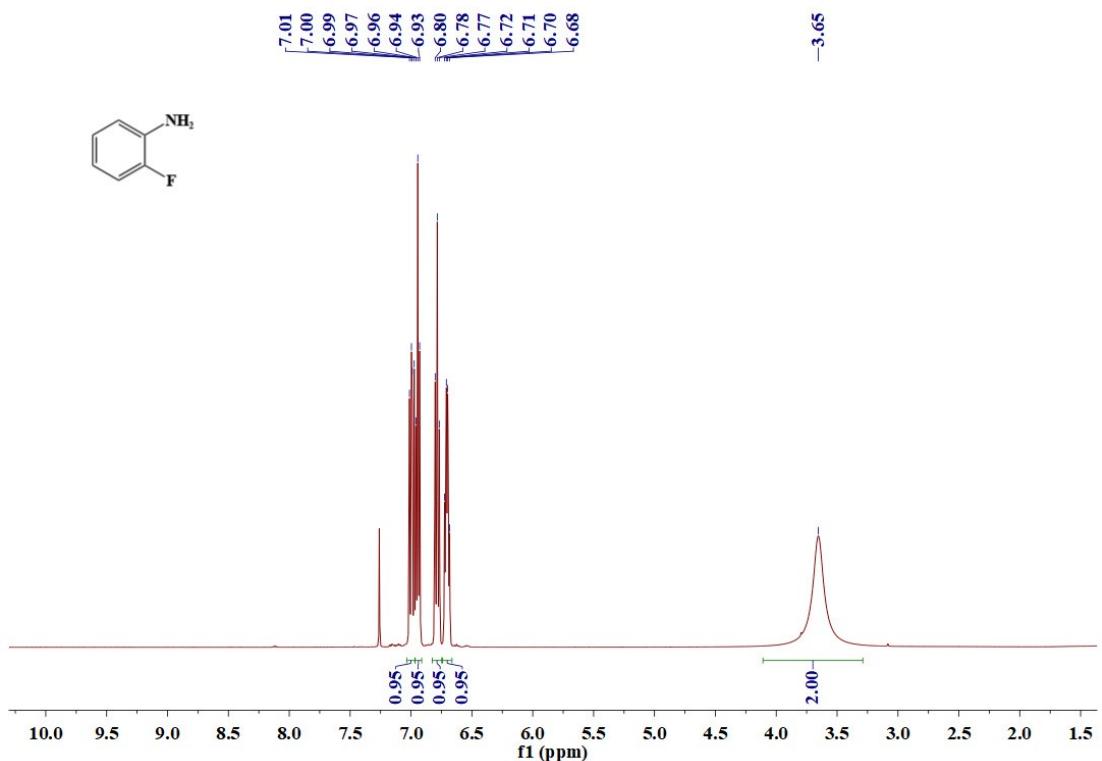
Figure S12. ^{1}H NMR spectra of **2-Fluoroaniline** (500 MHz, CDCl$_3$).

^{1}H (500 MHz, CDCl$_3$) δ 6.99 (dd, J = 11.3, 8.2 Hz, 1H), 6.94 (t, J = 7.6 Hz, 1H), 6.78 (t, J = 8.4 Hz, 1H), 6.70 (dd, J = 12.7, 7.6 Hz, 1H), 3.65 (s, 2H).
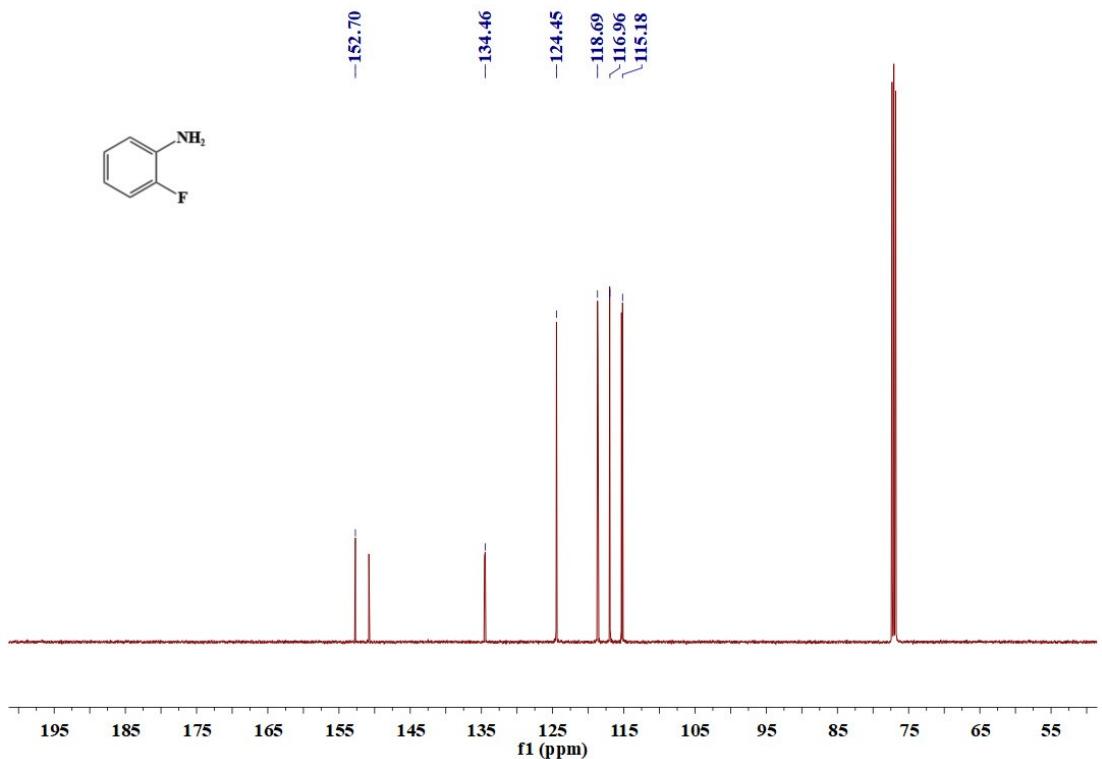
Figure S13. ^{13}C NMR spectra of **2-Fluoroaniline** (126 MHz, CDCl$_3$).

^{13}C NMR (126 MHz, CDCl$_3$) δ 152.70 (s), 134.46 (s), 124.45 (s), 118.69 (s), 116.96 (s), 115.18 (s).
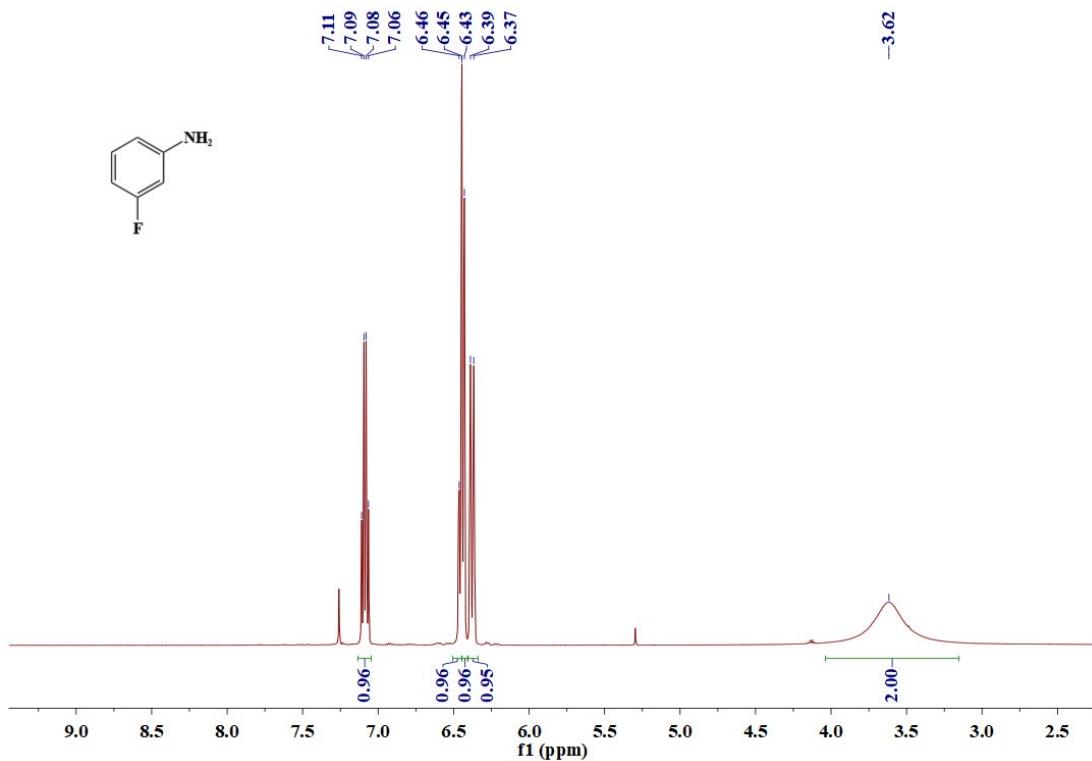
Figure S14. ^{1}H NMR spectra of **3-Fluoroaniline** (500 MHz, CDCl$_3$).

^{1}H (500 MHz, CDCl$_3$) δ 7.09 (dd, J = 15.0, 7.8 Hz, 1H), 6.45 (d, J = 8.9 Hz, 1H), 6.43 (s, 1H), 6.38 (d, J = 10.9 Hz, 1H), 3.62 (s, 2H)
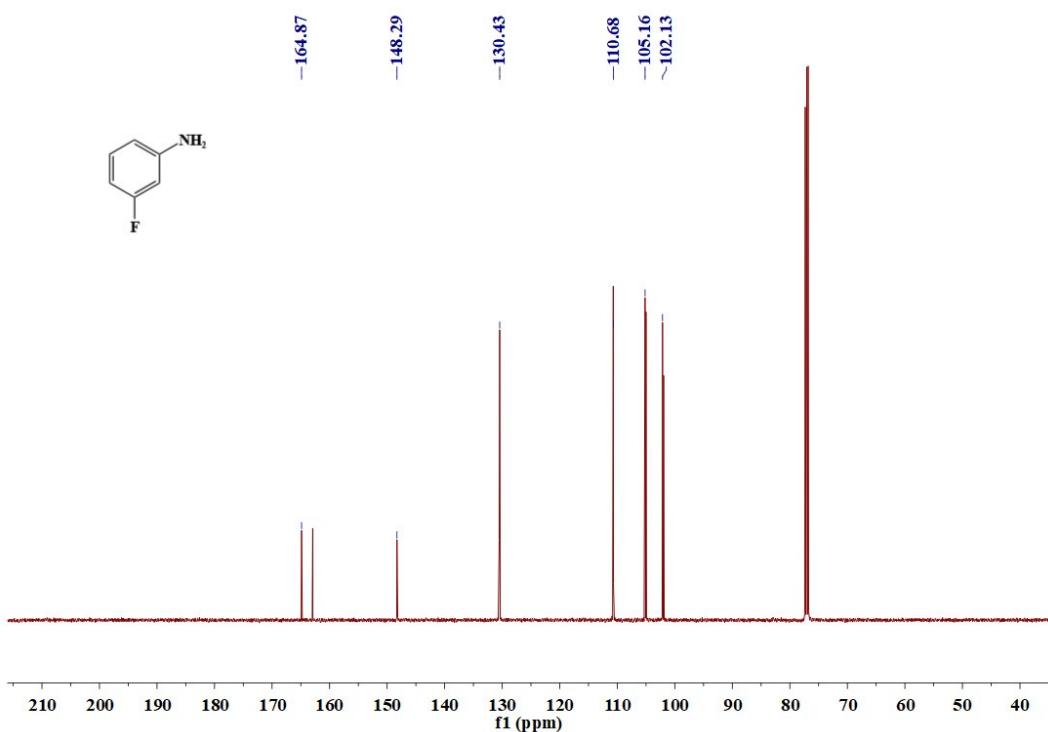
Figure S15. ^{13}C NMR spectra of **3-Fluoroaniline** (126 MHz, CDCl$_3$).

^{13}C NMR (126 MHz, CDCl$_3$) δ 164.87 (s), 148.29 (s), 130.43 (s), 110.68 (s), 105.16 (s), 102.13 (s).

S-21
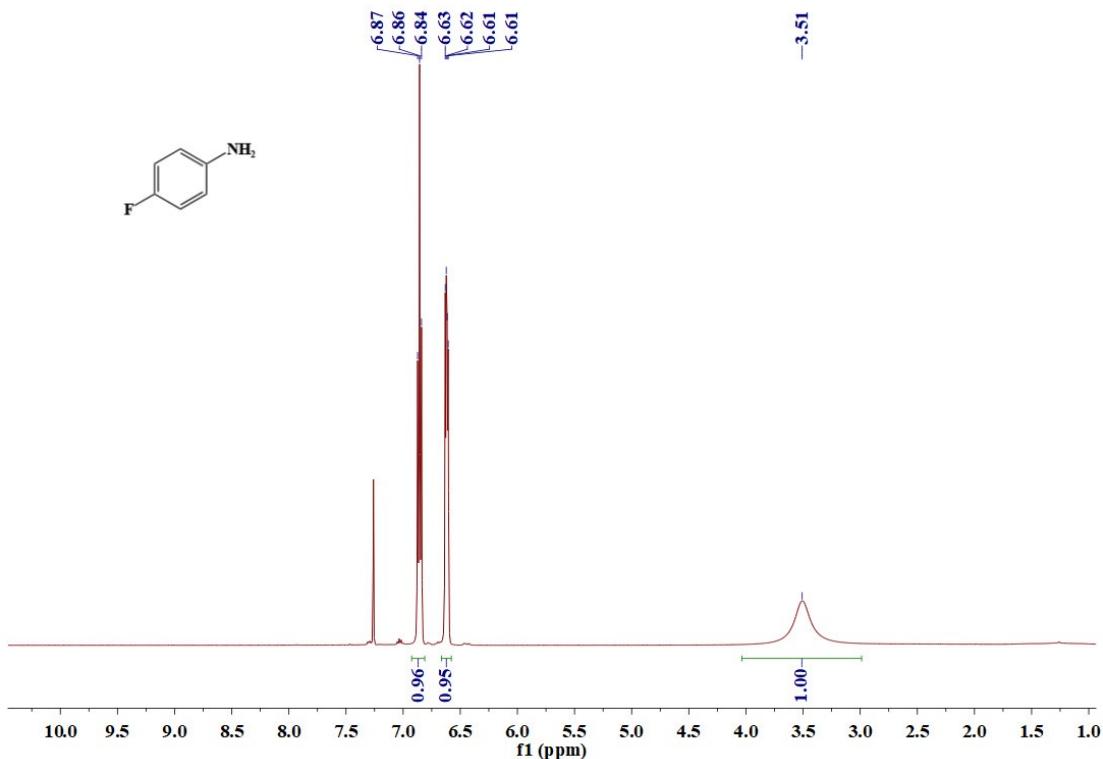
Figure S16. ^{1}H NMR spectra of **4-Fluoroaniline** (500 MHz, CDCl$_3$).

^{1}H (500 MHz, CDCl$_3$) δ 6.86 (t, J = 8.6 Hz, 2H), 6.62 (dd, J = 8.7, 4.4 Hz, 2H), 3.51 (s, 2H).
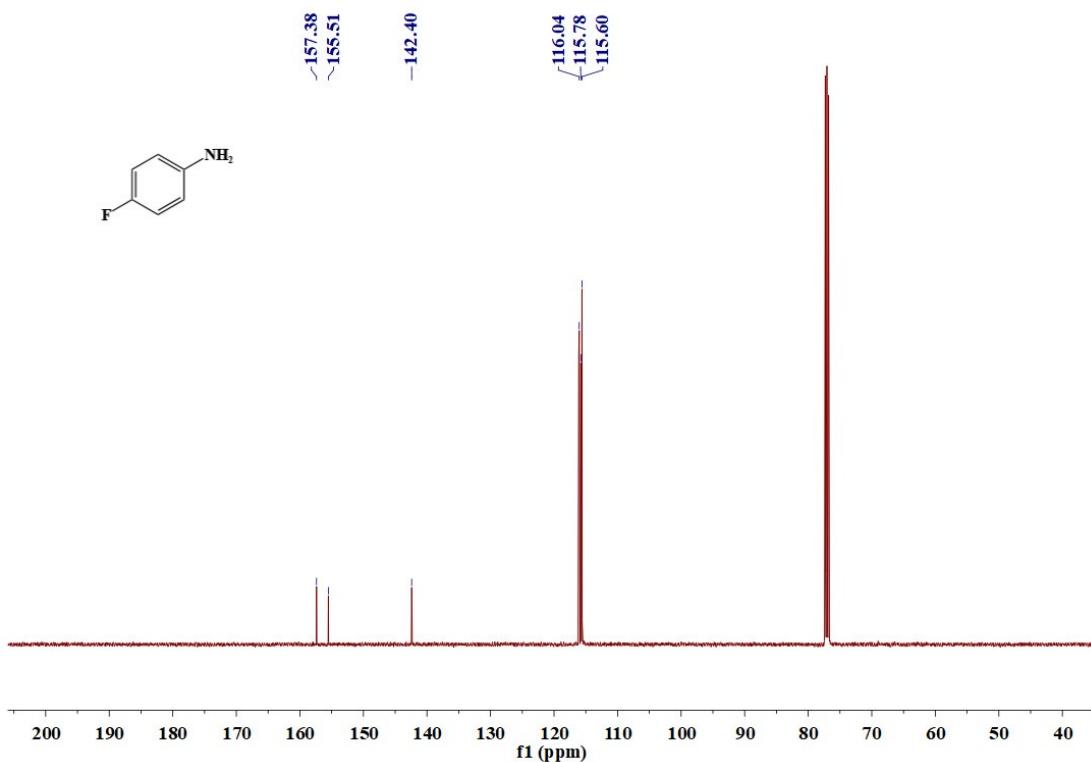
Figure S17. ^{13}C NMR spectra of **4-Fluoroaniline** (126 MHz, CDCl$_3$).

^{13}C NMR (126 MHz, CDCl$_3$) δ 157.38 (s), 155.51 (s), 142.40 (s), 116.04 (s), 115.78 (s), 115.60 (s)
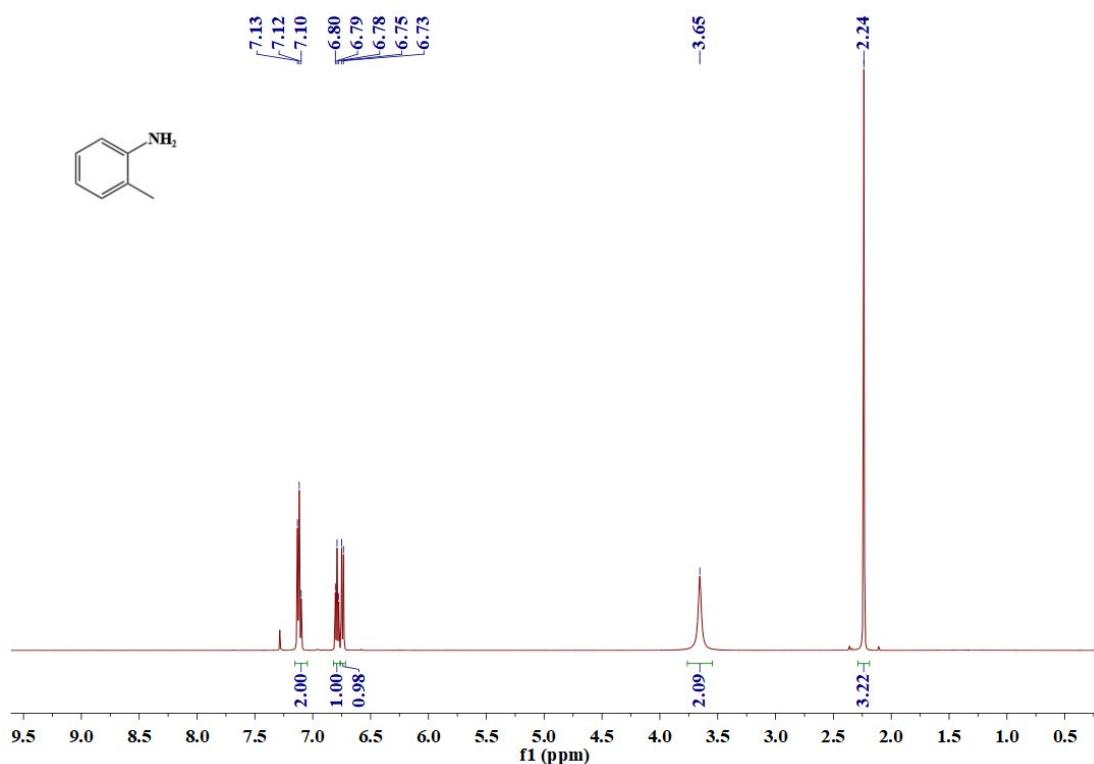
Figure S18. ^{1}H NMR spectra of **o-Toluidine** (500 MHz, CDCl$_3$).

^{1}H (500 MHz, CDCl$_3$) δ 7.12 (t, J = 8.1 Hz, 2H), 6.79 (t, J = 7.4 Hz, 1H), 6.74 (d, J = 7.7 Hz, 1H), 3.65 (s, 2H), 2.24 (s, 3H).
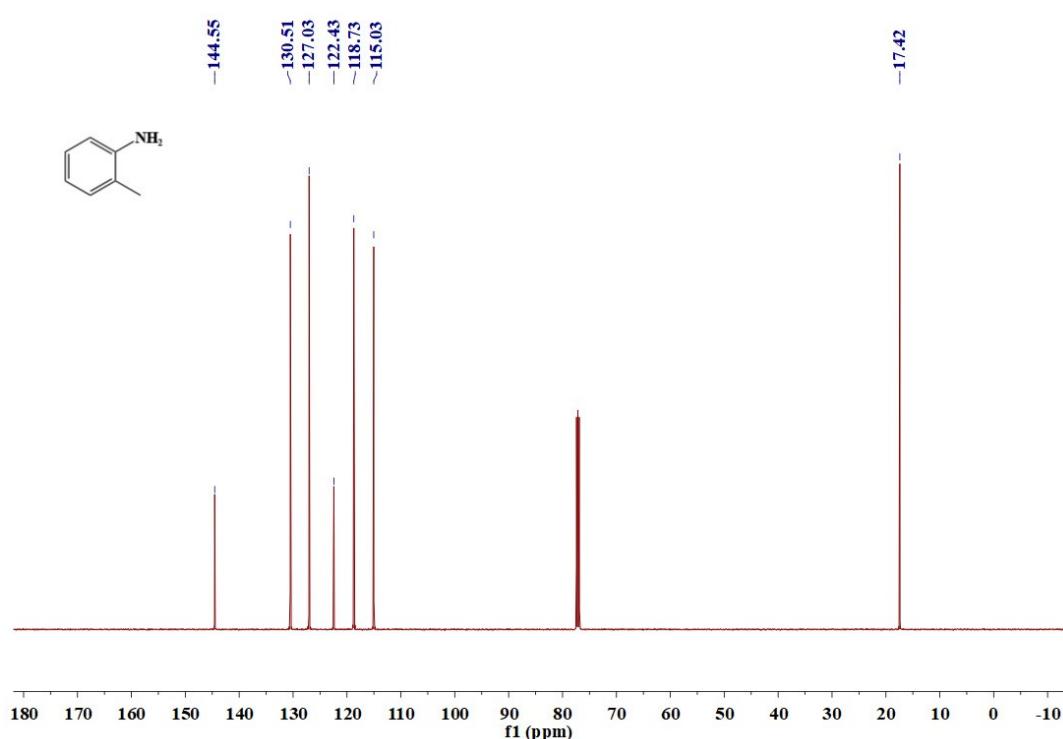
Figure S19. ^{13}C NMR spectra of **o-Toluidine** (126 MHz, CDCl$_3$).

^{13}C NMR (126 MHz, CDCl$_3$) δ 144.55 (s), 130.51 (s), 127.03 (s), 122.43 (s), 118.73 (s), 115.03 (s), 17.42 (s).
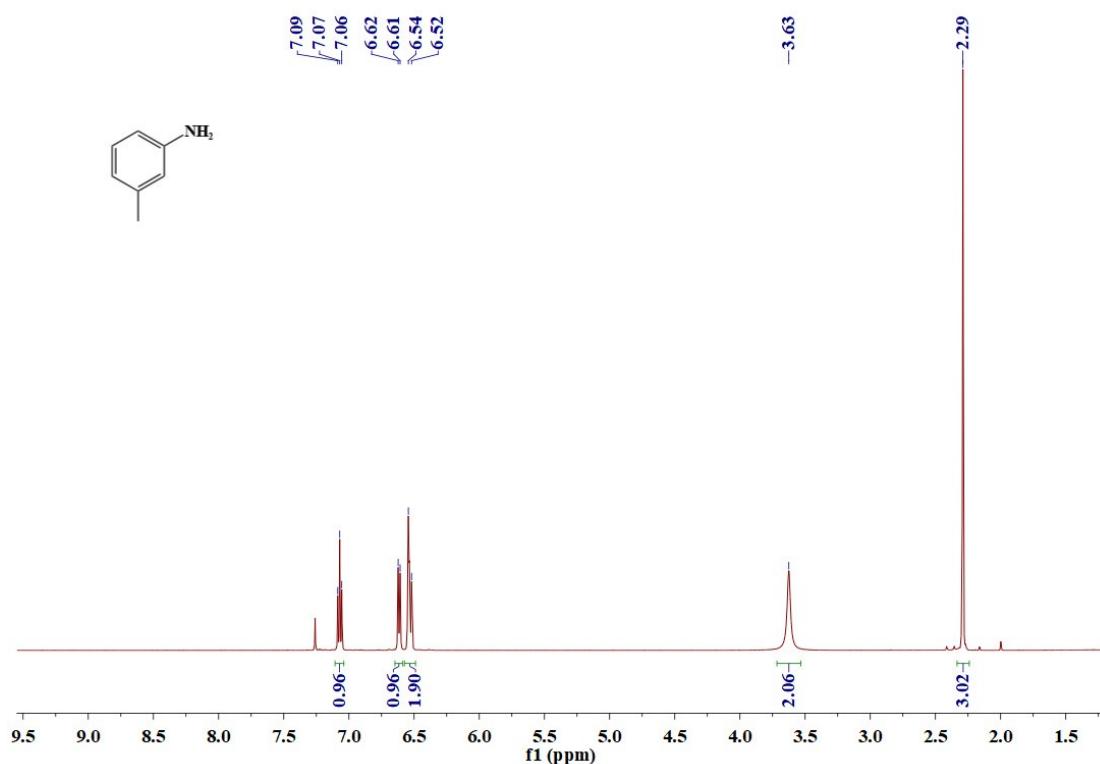
Figure S20. ^{1}H NMR spectra of **m-Toluidine** (500 MHz, CDCl$_3$).

[1]H (500 MHz, CDCl$_3$) δ 7.07 (t, J = 7.6 Hz, 1H), 6.61 (d, J = 7.5 Hz, 1H), 6.53 (d, J = 12.3 Hz, 2H), 3.63 (s, 2H), 2.29 (s, 3H).
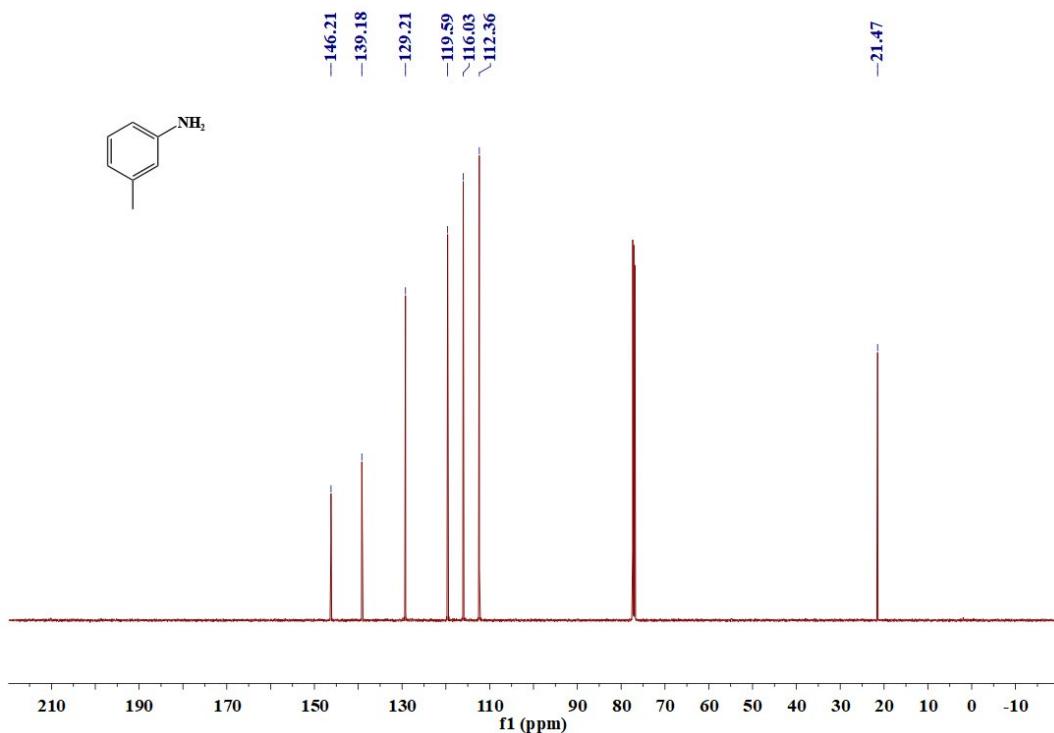

Figure S21. ^{13}C NMR spectra of **m-Toluidine** (126 MHz, CDCl$_3$).

^{13}C NMR (126 MHz, CDCl$_3$) δ 146.21 (s), 139.18 (s), 129.21 (s), 119.59 (s), 116.03 (s), 112.36 (s), 21.47 (s).
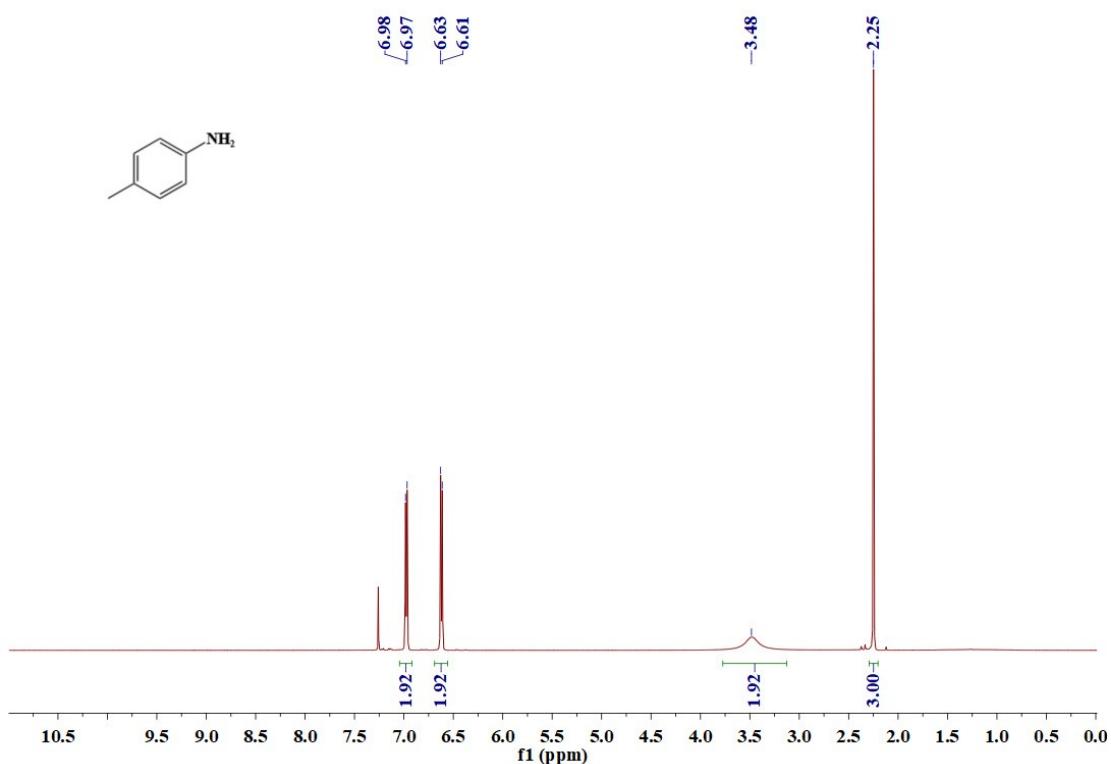
Figure S22. ¹H NMR spectra of **p-Toluidine** (500 MHz, CDCl₃).

¹H (500 MHz, CDCl₃) δ 6.98 (d, J = 8.0 Hz, 2H), 6.62 (d, J = 8.0 Hz, 2H), 3.48 (s, 2H), 2.25 (s, 3H).
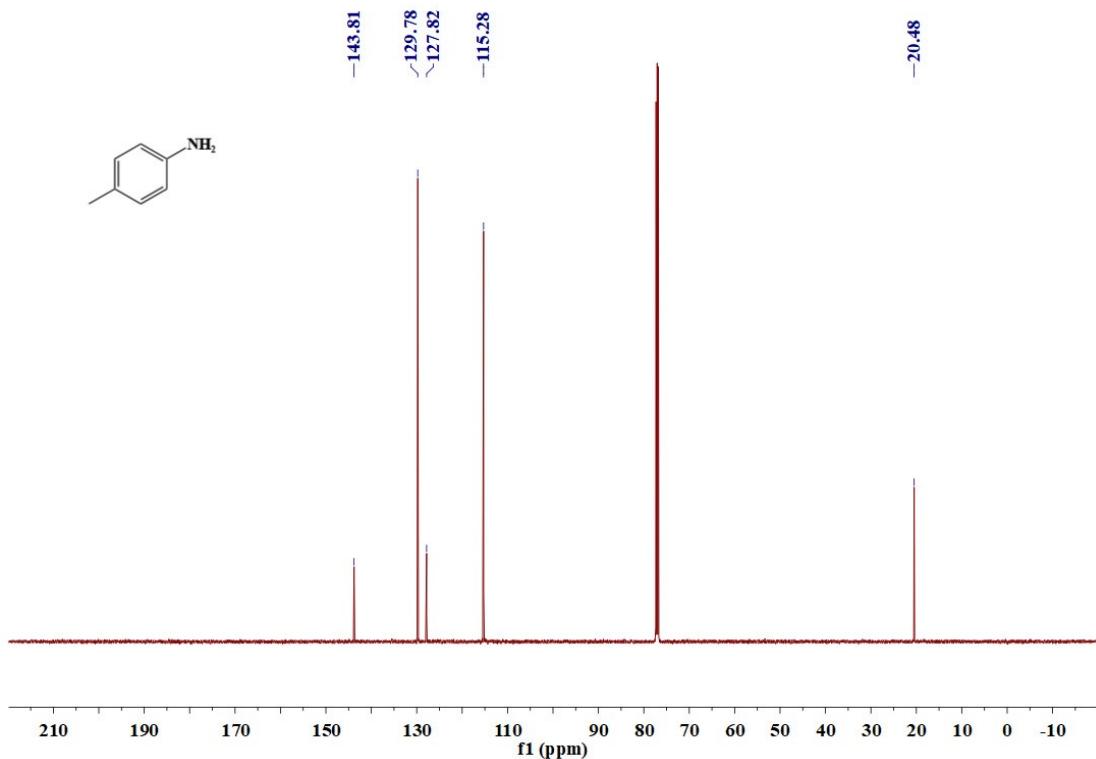
Figure S23. ¹³C NMR spectra of **p-Toluidine** (126 MHz, CDCl₃).

¹³C NMR (126 MHz, CDCl₃) δ 143.81 (s), 129.78 (s), 127.82 (s), 115.28 (s), 20.48 (s).
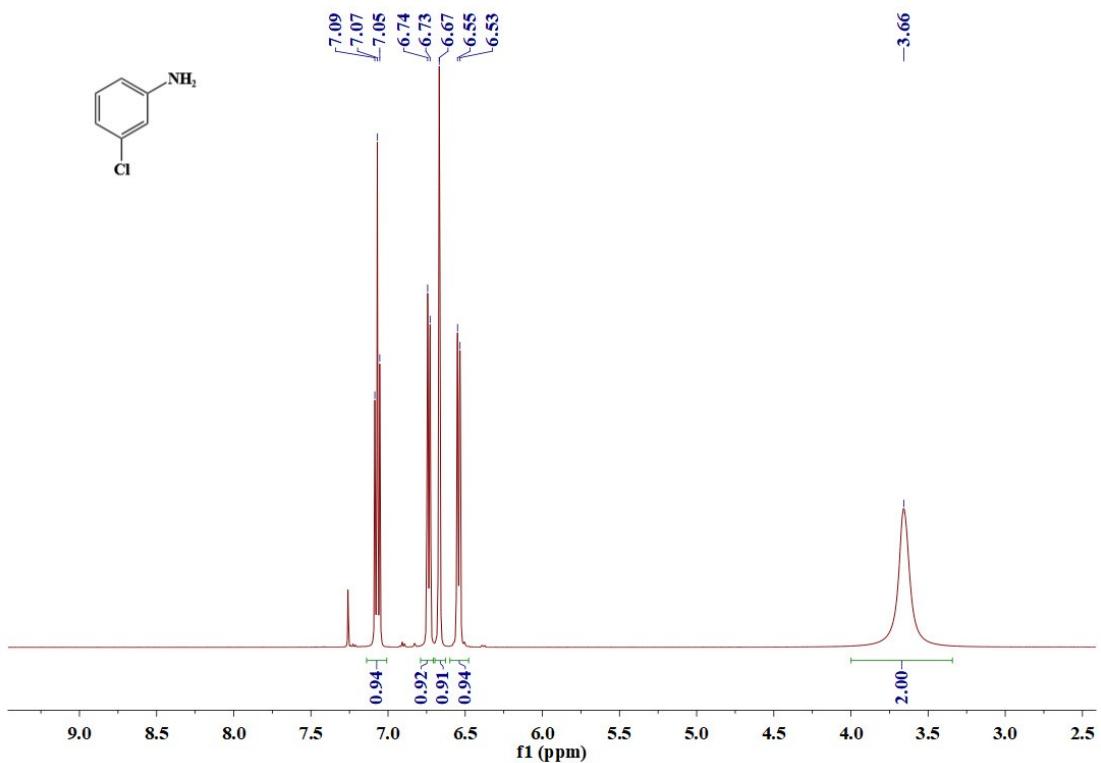
Figure S24. ¹H NMR spectra of **3-Chloroaniline** (500 MHz, CDCl₃).

¹H (500 MHz, CDCl₃) δ 7.07 (t, J = 8.0 Hz, 1H), 6.74 (d, J = 8.0 Hz, 1H), 6.67 (s, 1H), 6.54 (d, J = 8.1 Hz, 1H), 3.66 (s, 2H).
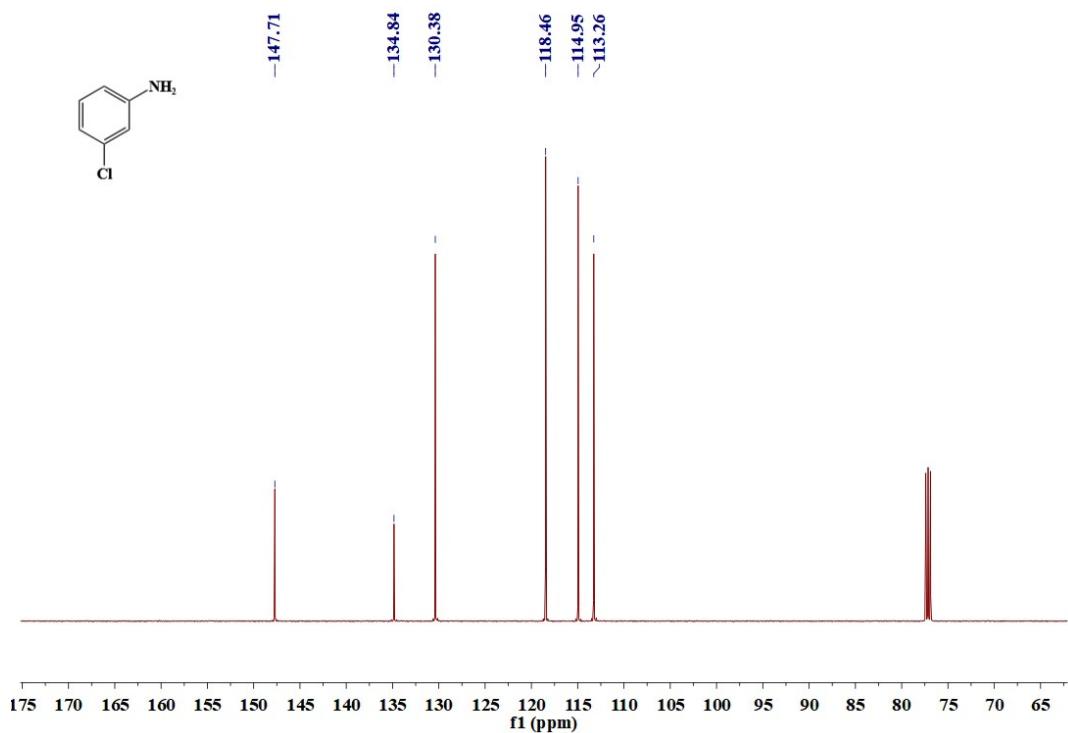

Figure S25. ¹³C NMR spectra of **3-Chloroaniline** (126 MHz, CDCl₃).

¹³C NMR (126 MHz, CDCl₃) δ 147.71 (s), 134.84 (s), 130.38 (s), 118.46 (s), 114.95 (s), 113.26 (s).
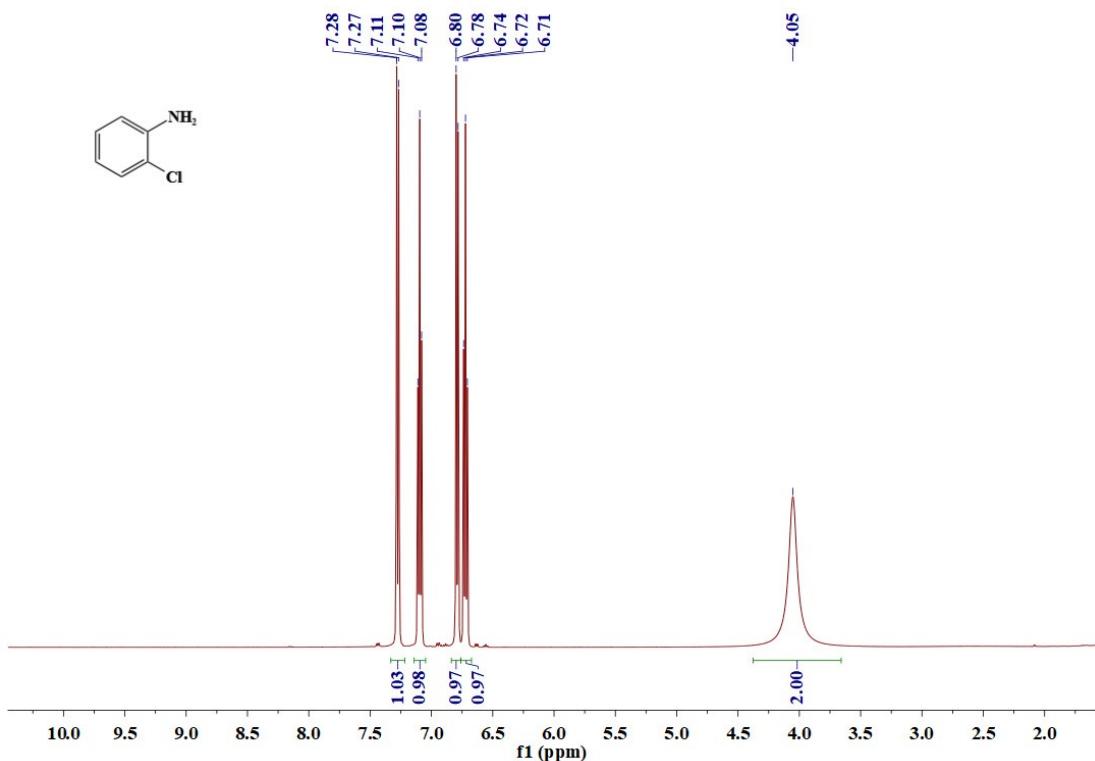
Figure S26. ^{1}H NMR spectra of **2-Chloroaniline** (500 MHz, CDCl$_3$).

^{1}H (500 MHz, CDCl$_3$) δ 7.27 (d, J = 8.1 Hz, 1H), 7.10 (t, J = 7.7 Hz, 1H), 6.79 (d, J = 8.0 Hz, 1H), 6.72 (t, J = 7.6 Hz, 1H), 4.05 (s, 2H).
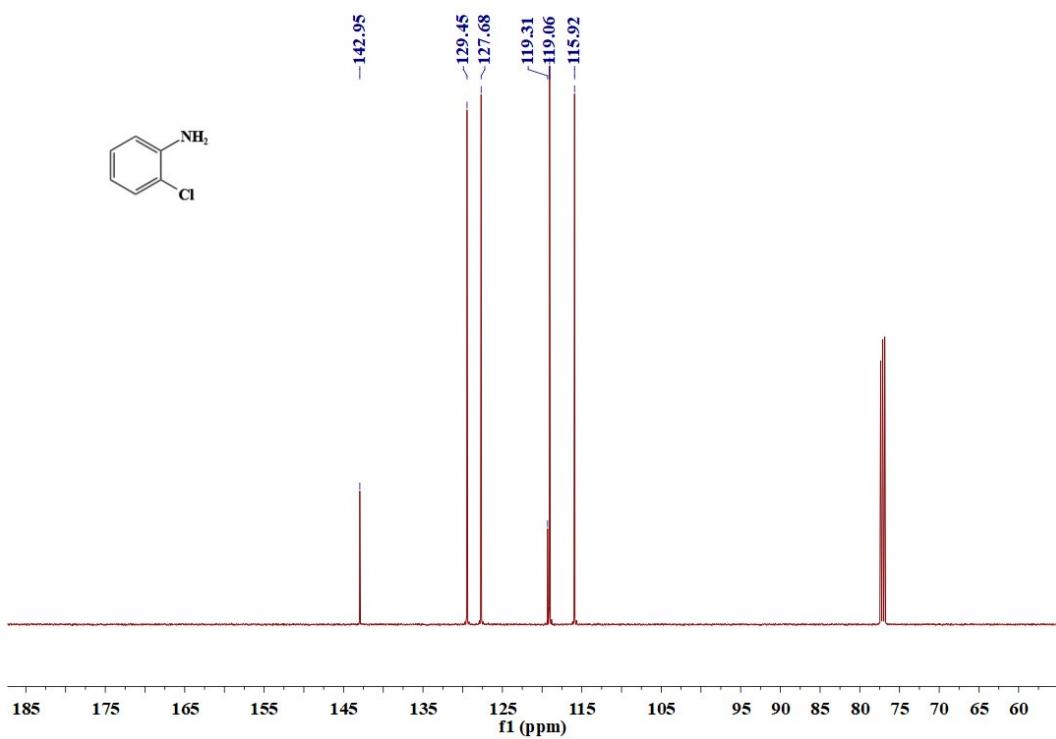
**Figure S27.** ^{13}C NMR spectra of **2-Chloroaniline** (126 MHz, CDCl$_3$).

^{13}C NMR (126 MHz, CDCl$_3$) δ 142.95 (s), 129.45 (s), 127.68 (s), 119.31 (s), 119.06 (s), 115.92 (s).
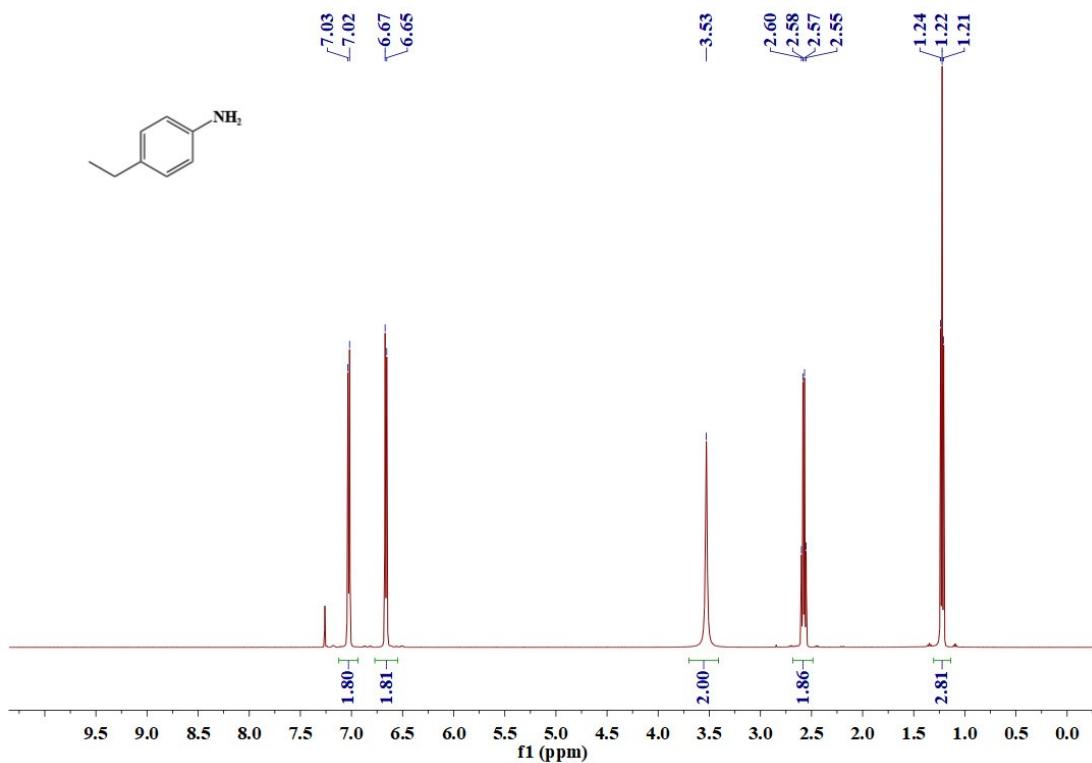
Figure S28. ^{1}H NMR spectra of **4-Ethylaniline** (500 MHz, CDCl$_3$).

^{1}H (500 MHz, CDCl$_3$) δ 7.03 (d, J = 8.1 Hz, 2H), 6.66 (d, J = 8.2 Hz, 2H), 3.53 (s, 2H), 2.58 (q, J = 7.6 Hz, 2H), 1.22 (t, J = 7.6 Hz, 3H).
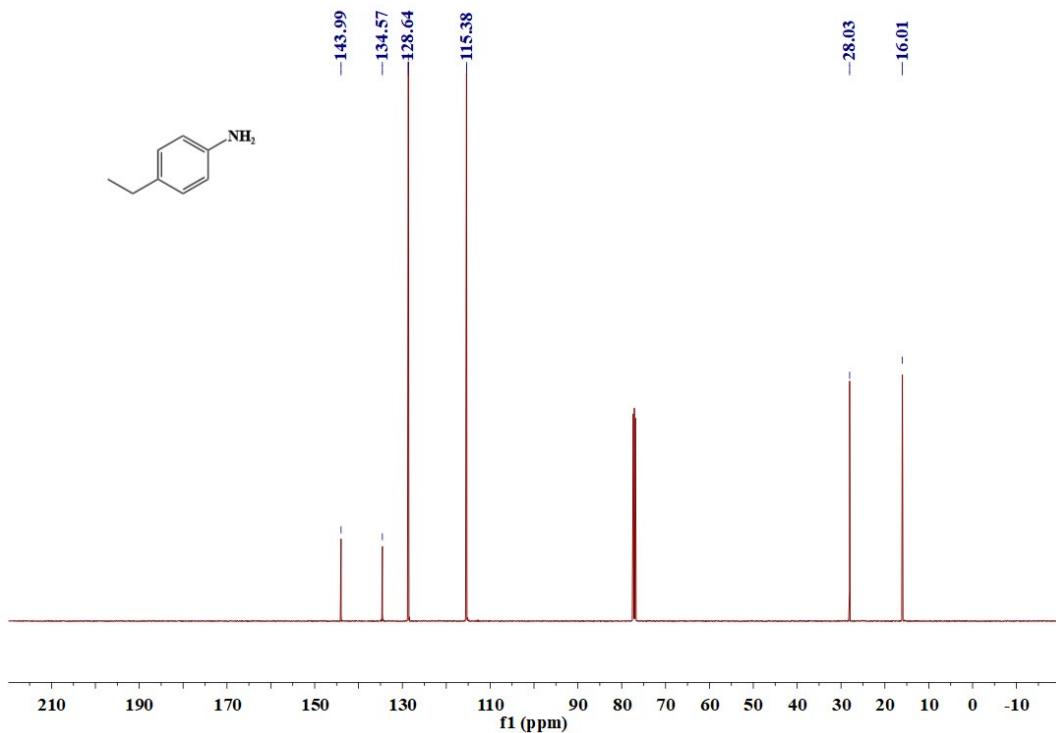
**Figure S29.** ^{13}C NMR spectra of **4-Ethylaniline** (126 MHz, CDCl$_3$).

^{13}C NMR (126 MHz, CDCl$_3$) δ 143.99 (s), 134.57 (s), 128.64 (s), 115.38 (s), 28.03 (s), 16.01 (s).
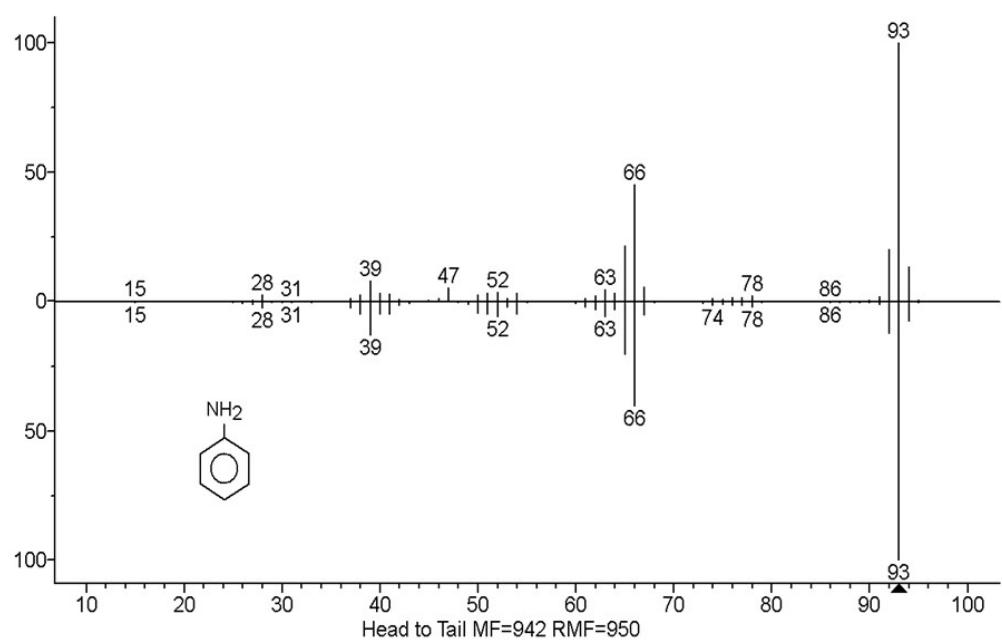
Figure S30. The GC-MS spectrum of aniline (bottom, simulation; top, experiment)

References

1 G. M. Sheldrick, *Acta Cryst A*, 2008, **64**, 112–122.

2 O. V. Dolomanov, L. J. Bourhis, R. J. Gildea, J. A. K. Howard and H. Puschmann, *J Appl Crystallogr*, 2009, **42**, 339–341.

3 R. Wan, Z. Liu, X. Ma, H. Li, P. Ma, C. Zhang, J. Niu and J. Wang, *Chem. Commun.*, 2021, **57**, 2172–2175.

4 B. Yan, Y. Li, S. R. Calhoun, N. G. Cottrell, D. J. Lella and A. J. Celestian, *Inorganic Chemistry Communications.*, 2014, **43**, 23–26.

5 X.-X. Li, C.-H. Li, M.-J. Hou, B. Zhu, W.-C. Chen, C.-Y. Sun, Y. Yuan, W. Guan, C. Qin, K.-Z. Shao, X.-L. Wang and Z.-M. Su, *Nat Commun.*, 2023, **14**, 5025.

6 S. Li, H. Wang, H. Su, H. Chen, M. Du, L. Long, X. Kong and L. Zheng, *Small Methods.*, 2021, **5**, 2000777.

7 H.-Y. Wang, S.-R. Li, X. Wang, L.-S. Long, X.-J. Kong and L.-S. Zheng, *Sci. China Chem.*, 2021, **64**, 959–963.

8 M. Zhu, T. Iwano, M. Tan, D. Akutsu, S. Uchida, G. Chen and X. Fang, *Angew Chem Int Ed.*, 2022, **61**, e202200666.

9 K. Niinomi, S. Miyazawa, M. Hibino, N. Mizuno and S. Uchida, *Inorg. Chem.*, 2017, **56**, 15187–15193.

10 S.-L. Yang, G. Li, M.-Y. Guo, W.-S. Liu, R. Bu and E.-Q. Gao, *J. Am. Chem. Soc.*, 2021, **143**, 8838–8848.

11 J. Chen, Q. Mei, Y. Chen, C. Marsh, B. An, X. Han, I. P. Silverwood, M. Li, Y. Cheng, M. He, X. Chen, W. Li, M. Kippax-Jones, D. Crawshaw, M. D. Frogley, S. J. Day, V. García-Sakai, P. Manuel, A. J. Ramirez-Cuesta, S. Yang and M. Schröder, *J. Am. Chem. Soc.*, 2022, **144**, 11969–11974.

12 L. Hao, S. Jia, X. Qiao, E. Lin, Y. Yang, Y. Chen, P. Cheng and Z. Zhang, *Angew. Chem. Int. Ed.*, 2023, **62**, e202217240.

13 G. Jiang, W. Zou, Z. Ou, L. Zhang, W. Zhang, X. Wang, H. Song, Z. Cui, Z. Liang and L. Du, *Angew. Chem. Int. Ed.*, 2022, **61**, e202208086.

14 S. Chen, Y. Ju, H. Zhang, Y. Zou, S. Lin, Y. Li, S. Wang, E. Ma, W. Deng, S. Xiang, B. Chen and Z. Zhang, *Angew Chem Int Ed.*, 2023, **62**, e202308418.

15 W.-W. Wu, B. Li, M.-M. Wang, J.-J. Cai, S. Andra, H.-J. Lun, Y. Bai, D.-B. Dang and Y.-M. Li, *Chem. Mater.*, 2023, **35**, 6549–6556.

16 W. Chen, H. Li, Y. Jin, C. Wu, Z. Yuan, P. Ma, J. Wang and J. Niu, *Chem. Commun.*, 2022, **58**, 9902–9905.

17 W. Tang, Y. Liu, Y. Jin, Y. Wang, W. Shi, P. Ma, J. Niu and J. Wang, *Inorg. Chem.*, 2024, **63**, 6260–6267.

18 J. Jiao, H. Sun, C. Si, J. Xu, T. Zhang and Q. Han, *ACS Appl. Mater. Interfaces*, 2022, **14**, 16386–16393.

19 T. Zhang, C. Si, K. Guo, X. Liu, Q. Liu, J. Fu and Q. Han, *Inorg. Chem.*, 2022, **61**, 20657–20665.

20 C. Si, F. Liu, X. Yan, J. Xu, G. Niu and Q. Han, *Inorg. Chem.*, 2022, **61**, 5335–5342.

21 S.-K. Shi, X. Li, H. Guo, Y. Fan, H. Li, D.-B. Dang and Y. Bai, *Inorg. Chem.*, 2020, **59**, 11213–11217.